nature communications

Article

https://doi.org/10.1038/s41467-024-53909-8

Sulfate residuals on Ru catalysts switch CO_2 reduction from methanation to reverse water-gas shift reaction

Received: 7 March 2024

Accepted: 25 October 2024

Published online: 02 November 2024

Check for updates

Min Chen[1], Longgang Liu[2], Xueyan Chen[1], Xiaoxiao Qin[1], Jianghao Zhang[1], Shaohua Xie[3], Fudong Liu[3] ✉, Hong He[1,4] & Changbin Zhang[1,4] ✉

Efficient heterogeneous catalyst design primarily focuses on engineering the active sites or supports, often neglecting the impact of trace impurities on catalytic performance. Herein, we demonstrate that even trace amounts of sulfate (SO_4^{2-}) residuals on Ru/TiO_2 can totally change the CO_2 reduction from methanation to reverse-water gas shift (RWGS) reaction under atmospheric pressure. We reveal that air annealing causes the trace amount of SO_4^{2-} to migrate from TiO_2 to Ru/TiO_2 interface, leading to the significant changes in product selectivity from CH_4 to CO. Detailed characterizations and DFT calculations show that the sulfate at Ru/TiO_2 interface notably enhances the H transfer from Ru particles to the TiO_2 support, weakening the CO intermediate activation on Ru particles and inhibiting the further hydrogenation of CO to CH_4. This discovery highlights the vital role of trace impurities in CO_2 hydrogenation reaction, and also provides broad implications for the design and development of more efficient and selective heterogeneous catalysts.

At present, the atmospheric CO_2 level has surged to a historically high of approximately 416 ppm, further reinforcing the existing concerns about its significant contribution to global climate change[1–4]. Long treated as waste, CO_2 is now considered as a potentially useful carbon source for producing fuels and chemicals through photocatalytic, electrocatalytic, and thermal catalytic reduction in the presence of H_2, which can be obtained from water splitting using solar, wind, or other renewable energy sources[5–8]. Thermal catalytic reduction typically offers high reaction efficiency and is extensively used in practical applications. By designing supported metal catalysts and controlling the reaction conditions, a wide range of products, such as methane (CH_4)[9–11], carbon monoxide (CO)[12,13], methanol (CH_3OH)[14,15], and even long-chain hydrocarbons can be obtained[16].

Catalytic hydrogenation of CO_2 at atmospheric pressure typically involves either methanation reaction, yielding CH_4, or reverse water-gas shift (RWGS) reaction, leading to CO production[1,2,16–19]. Both methanation and RWGS reactions play crucial roles in industrial processes related to hydrogen utilization and synthesis gas production. CO_2 hydrogenation to CH_4 or CO with high selectivity is desired according to specific application requirements but remains challenging. Previous research has established that the supported Ru/TiO_2 catalysts are one of the most active and stable catalysts in CO_2 hydrogenation reaction[20–22]. Very recently, some reports have highlighted that the crystal structure of TiO_2 support significantly impacted the selectivity of CO_2 hydrogenation on Ru/TiO_2 catalysts[18,23–25]. Qiao at al. observed that the selectivity of CO_2 hydrogenation could be completely reversed when Ru particles were supported on anatase-TiO_2 (high CO selectivity) versus on rutile-TiO_2 (high CH_4 selectivity)[23]. This phenomenon was attributed to the different electron transfer processes from Ru to the TiO_2 supports as a result of varying extents of hydrogen spillover related to crystal structure[23]. Wang et al. reported that annealing Ru/rutile-TiO_2 in air enhanced the CO_2 conversion to

[1]State Key Joint Laboratory of Environment Simulation and Pollution Control, Research Center for Eco-Environmental Sciences, Chinese Academy of Sciences, Beijing, China. [2]School of Chemistry and Chemical Engineering, Qufu Normal University, Qufu, China. [3]Department of Chemical and Environmental Engineering, Bourns College of Engineering, Center for Environmental Research and Technology (CE-CERT), Materials Science and Engineering (MSE) Program, University of California, Riverside, CA, USA. [4]University of Chinese Academy of Sciences, Beijing, China. ✉e-mail: fudong.liu@ucr.edu; cbzhang@rcees.ac.cn

CH_4, while annealing Ru/anatase-TiO_2 in air decreased the CO_2 conversion and led to CO production. They ascribed these differences to the contrasting metal-support interaction between Ru and anatase or rutile[18]. In contrast, Debecker et al. found that Ru supported on anatase, rutile, or a mixture of the two exhibited a variety of CO_2 conversions, but high CH_4 selectivity was observed on all catalysts[24]. The disparity in the observed CO or CH_4 selectivity among researchers indicates that the crystal structure of TiO_2 supports may not be the sole determining factor for the catalytic performance of CO_2 hydrogenation.

Upon careful examination of the literatures mentioned above, we noticed that the TiO_2 supports used in these studies were usually obtained from commercial sources, with some samples possibly containing trace amounts of residual impurities. Some impurities might remarkably affect the catalytic performance of Ru catalysts in CO_2 hydrogenation; however, their distinct significance was often overlooked in the course of research, potentially leading to flawed conclusions. In this work, we observed that the typical Ru/TiO_2 catalysts using both anatase and rutile supports displayed excellent performance in CO_2 methanation reaction. Surprisingly, the Ru/TiO_2 catalysts containing trace amount of SO_4^{2-} residuals showed no activity in CO_2 methanation, but excellent activity in RWGS reaction. This unique phenomenon suggested that the SO_4^{2-} residuals on these Ru catalysts, rather than the crystal structure of the TiO_2 supports, plays the key role in determining the catalytic performance of CO_2 hydrogenation. Further investigation revealed that annealing the sulfate-containing Ru/TiO_2 in air induced the sulfate migration from the TiO_2 support to the Ru/TiO_2 interface. At the interface, the sulfate could strongly promote the transfer of hydrogen from Ru particles to the TiO_2 support. The enhanced hydrogen spillover weakened the activation of CO intermediates on Ru particles, leading to significantly higher selectivity for CO production. This work not only introduces a novel viewpoint for elucidating the variation of observed CO or CH_4 selectivity of CO_2 hydrogenation on Ru/TiO_2 catalysts, but also leads to a fundamental guideline for new catalyst design including the careful control of impurity levels and exploiting their positive impacts.

Results

The effects of sulfate on the catalytic performance of Ru/TiO_2 for CO_2 hydrogenation

A set of Ru/TiO_2 catalysts (with anatase TiO_2 purchased from Aldrich or Aladdin) were prepared by a wet impregnation method, with the Ru loading of 5 wt.%. The catalytic reduction of CO_2 was conducted at atmospheric pressure within the temperature range from 200 to 450 °C, in a fixed-bed flow reactor with a gas mixture composed of CO_2 (10 vol.%), H_2 (40 vol.%), and N_2 balance. The gas weight hourly space velocity (WHSV) was approximately 48,000 mL·g^{-1}·h^{-1}. The CO_2 hydrogenation under these conditions typically yields CH_4 via CO_2 methanation reaction and CO via RWGS reaction. Moreover, CO_2 methanation is more thermodynamically favorable compared to the RWGS reaction when the reaction temperature is below 500 °C[26]. Our calculation results about the thermodynamic equilibrium of CO_2 hydrogenation also showed that CH_4 was the favored product at lower temperature (<500 °C), while CO was the favored product at higher temperature (>500 °C) (Supplementary Figs. 1, 2). Thus, it remains an ongoing challenge to tune the high CH_4 selectivity to high CO selectivity at lower temperatures.

Figure 1a illustrates the products comparison on different sets of Ru/TiO_2 catalysts (the detailed comparison is provided in Supplementary Fig. 3). CH_4 was the main product on some Ru/TiO_2 catalysts, while CO was the main product on other Ru/TiO_2 catalysts. Considering that the purchased anatase TiO_2 supports may contain trace amount of sulfate species as impurity, we conducted the element analysis by inductively coupled plasma mass spectrometry (ICP-MS,

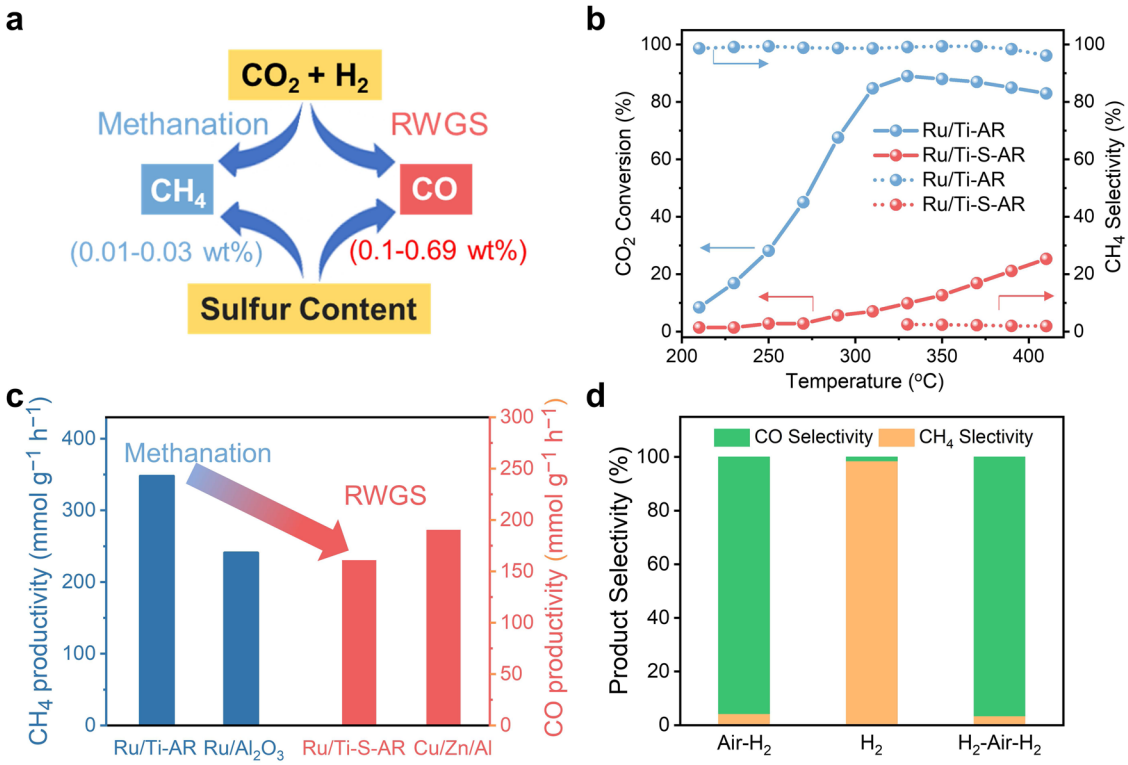

Fig. 1 | Catalytic performance of the Ru/TiO_2 catalysts. a The products and sulfur content comparison on the different sets of Ru/TiO_2 catalysts for CO_2 hydrogenation. **b** Temperature-dependent CO_2 conversion and CH_4 selectivity of Ru/TiO_2 catalysts with or without SO_4^{2-} species. **c** Comparison with commercial Ru/Al_2O_3 catalyst for CH_4 productivity at 350 °C and commercial CuO/ZnO/Al_2O_3 catalyst for CO productivity at 410 °C. **d** The product selectivity on Ru/Ti-S catalyst with air and/or H_2 pretreatment at 350 °C.

see Supplementary Table 1). The results revealed that these TiO_2 supports could be divided into two groups, with one group showing nearly no presence of SO_4^{2-} (i.e., very low S content of 0.01–0.03 wt.%) and the other group showing the presence of trace amount of SO_4^{2-} with relatively higher S content of 0.1–0.7 wt.%. Surprisingly, it was observed that the Ru/TiO_2 catalysts with no SO_4^{2-} displayed high CH_4 selectivity, while the Ru/TiO_2 catalysts with trace amount of SO_4^{2-} displayed high CO selectivity. These results strongly indicate that the presence of trace amount of SO_4^{2-} on Ru/TiO_2 may play a crucial role in impacting the selectivity of CO_2 hydrogenation reaction.

To further investigate the influence of SO_4^{2-} on the catalytic performance of CO_2 hydrogenation, we prepared the sulfate-free Ru/TiO_2 catalysts, in which the sulfate-free TiO_2 were synthesized by hydrolyzing tetrabutyl titanate, and also prepared the Ru/TiO_2 catalysts containing sulfate by purposely adding ammonium sulfate during the preparation process (with mole ratio of S/Ru set as 0, 0.03, 0.05, and 0.1). Before testing and characterization, the obtained sulfate-free and sulfated Ru/TiO_2 catalysts were annealed in air at 400 °C and then reduced by H_2 at 500 °C (denoted as Ru/Ti-AR and Ru/Ti-S-AR, Ru/Ti = Ru supported on anatase TiO_2, S = sulfated, AR = air annealing and H_2 reduction). Figure 1b shows that the Ru/Ti-AR exhibited excellent activity for CO_2 hydrogenation between 150 and 410 °C, and the CO_2 conversion reached the highest of *ca*. 89% at 330 °C and slightly decreased to 83% at 410 °C. The CH_4 selectivity maintained above 95% within this temperature range. With increasing the mole ratio of S/Ru from 0 to 0.1 (note that the ratio of S/Ru in Ru/Ti-S-AR was 0.1), the CO_2 conversion dropped sharply and the product distribution dramatically changed from CH_4 to CO (Supplementary Fig. 4). Besides, we tested the activity of the Ru/Ti-S-AR by altering contact time (Supplementary Fig. 5). The results showed that the CO_2 conversion was enhanced by increasing contact time, but high CO selectivity still remained, further confirming the high CO selectivity on Ru/Ti-S-AR. Compared with the commercial Ru/Al_2O_3 catalyst for CO_2 methanation and $CuO/ZnO/Al_2O_3$ catalyst for RWGS reaction (Fig. 1c), the CH_4 production on Ru/Ti-AR at 350 °C was 348 mmol g^{-1} h^{-1}, which was 1.4 times higher than that on Ru/Al_2O_3. The CO production on Ru/Ti-S-AR at 410 °C was 160 mmol g^{-1} h^{-1}, which was close to that on Cu/Zn/Al (191 mmol g^{-1} h^{-1}). These results suggest that the Ru/Ti-AR performed as an efficient catalyst for CO_2 methanation reaction, while the Ru/Ti-S-AR performed as an efficient catalyst for RWGS reaction.

Considering that the crystal structure of TiO_2 was frequently discussed in influencing the product selectivity on Ru/TiO_2 catalyst in CO_2 hydrogenation reaction, we also synthesized a series of Ru/rutile catalysts, including the sulfate-free Ru/rutile-AR and Ru/rutile-R, as well as the sulfate-containing Ru/rutile-S-AR and Ru/rutile-S-R (AR = air annealing and H_2 reduction, S = sulfated, R = direct H_2 reduction). Upon analyzing the testing results depicted in Supplementary Fig. 6, we observed the similar trends as that on Ru/Ti catalysts. In short summary, both the sulfate-free Ru/TiO_2 catalysts (using anatase or rutile as support) showed high CH_4 selectivity, while the sulfate-modified Ru/TiO_2 showed high CO selectivity. These results emphasized that the presence of sulfate residuals in TiO_2 support, rather than the crystal structure of TiO_2, was the key factor influencing the catalytic performance of CO_2 hydrogenation.

Pretreating catalysts under different atmospheres commonly impacted the performance of catalysts in many reactions. Figure 1d shows that the high CO selectivity on Ru/Ti-S-AR was observed at 350 °C by annealing the as-prepared Ru/Ti-S in air followed by H_2 reduction. The pretreatment condition was also switched to direct H_2 reduction without pre-annealing in air. Surprisingly, the high CH_4 selectivity was observed (Fig. 1d). Afterwards, this sample was further treated with air annealing and subsequent H_2 reduction, and the product selectivity could achieve high CO (see detailed activity results as shown in Supplementary Fig. 7). In contrast, when the as-prepared sulfate-free Ru/Ti was pretreated under similar conditions, no such switch of product selectivity was observed at all (Supplementary Fig. 8). These findings suggest that when there was trace amount of sulfate species on Ru/TiO_2 catalysts, annealing the catalysts in air was highly crucial for regulating the product selectivity in CO_2 hydrogenation.

Sulfate-induced structural modification of Ru/TiO_2

To understand the effect of sulfates on the structure of Ru/TiO_2 catalysts, we investigated the geometric states of Ru nanoparticles (NPs) on different samples. The Ru/TiO_2 catalysts were prepared using the traditional wet impregnation method, which typically resulted in a wide range of metal dispersion on the support. High-angle annular dark-field scanning transmission electron microscopy (HAADF-STEM) measurement of the Ru/Ti-S-AR catalyst revealed numerous Ru particles distributed on the TiO_2 support, with sizes ranging from 5 to 12 nm (average size of 5.7 nm) (Fig. 2a and Supplementary Fig. 9). The Ru/Ti-AR exhibited a similar size distribution of Ru particles to that of Ru/Ti-S-AR. As shown in Supplementary Fig. 10, the Ru size distribution on Ru/Ti-R was in the range of 1–7 nm, with an average size of 2.9 nm, which was also comparable to that on Ru/Ti-S-R. The sizes of Ru derived from HAADF-STEM were in good agreement with XRD data (Supplementary Fig. 12). A summary about the Ru particles size and dispersion was shown in Supplementary Table 2. These results suggested that the air annealing at high temperature followed by H_2 reduction led to a higher degree of Ru particle aggregation compared with direct H_2 reduction treatment, and the presence of sulfate had negligible influence on the Ru particle size distribution.

The distribution of sulfate species on Ru/Ti-S-AR and Ru/Ti-S-R was investigated using energy dispersive X-ray (EDX) mapping. As shown in Fig. 2b, d, the S element on Ru/Ti-S-AR tended to accumulate near Ru particles, while the sulfates on Ru/Ti-S-R were randomly distributed on Ru/Ti-S-R. The distribution pattern of Ru and S elements on Ru/Ti-S-R-AR was similar to that on Ru/Ti-S-AR (Supplementary Fig. 11). This distinct relationship between Ru and S element distribution suggested that the air annealing could effectively drive the migration of sulfates on TiO_2 to the Ru/TiO_2 interface. In general, the sulfate species are bonded with TiO_2 through the chemical bonding of Ti-S. However, when the Ru species are loaded on TiO_2, a stronger chemical bonding of Ru-S may be present. During the air annealing at high temperatures, the surface sulfates on TiO_2 likely migrated to the Ru/TiO_2 interface to form a more stable state with the stronger chemical bonding of Ru-S (as illustrated in Fig. 2e).

The spatial distribution of sulfates differed noticeably between Ru/Ti-S-R and Ru/Ti-S-AR, implying that the chemical states of sulfate species were also expected to be distinct. To prove this point-of-view, we performed X-ray photoelectron spectroscopy (XPS) measurement. The S $2p_{1/2}$ spectra between binding energies of 160–172 eV are shown in Fig. 3a. For both Ru/Ti-S-AR and Ru/Ti-S-R, the doublet peaks of S $2p_{1/2}$ were observed at 169.4 and 168.2 eV, corresponding to the presence of sulfate ions (SO_4^{2-})[27]. In addition, for Ru/Ti-S-AR, the peaks at 161.5 and 162.5 eV were detected, indicating the presence of S^{2-}[28], while these two peaks were considerably weaker for Ru/Ti-S-R. The presence of SO_4^{2-} could be attributed to the introduction of $(NH_4)_2SO_4$ during the preparation process. The SO_4^{2-} bonded on the surface of TiO_2, while the appearance of S^{2-} was indicative of the formation of Ru-S bonds, confirming that the air annealing indeed facilitated the migration of a certain amount of sulfate from the TiO_2 support to the Ru/TiO_2 interface.

H_2-temperature-programmed reduction (H_2-TPR) experiments were performed to investigate the reducibility of catalysts and the interactions at the metal-support interfaces. The H_2-TPR results (Fig. 3b) showed that all the samples exhibited two main reduction peaks, centered at 95–103 °C and 128–131 °C, corresponding to the reduction of surface RuO_x species weakly and strongly interacting with TiO_2, respectively[25,29,30]. The surface RuO_x species were typically reduced by H_2 easily, displaying peaks at lower temperatures (95–103 °C), whereas the interfacial RuO_x required higher

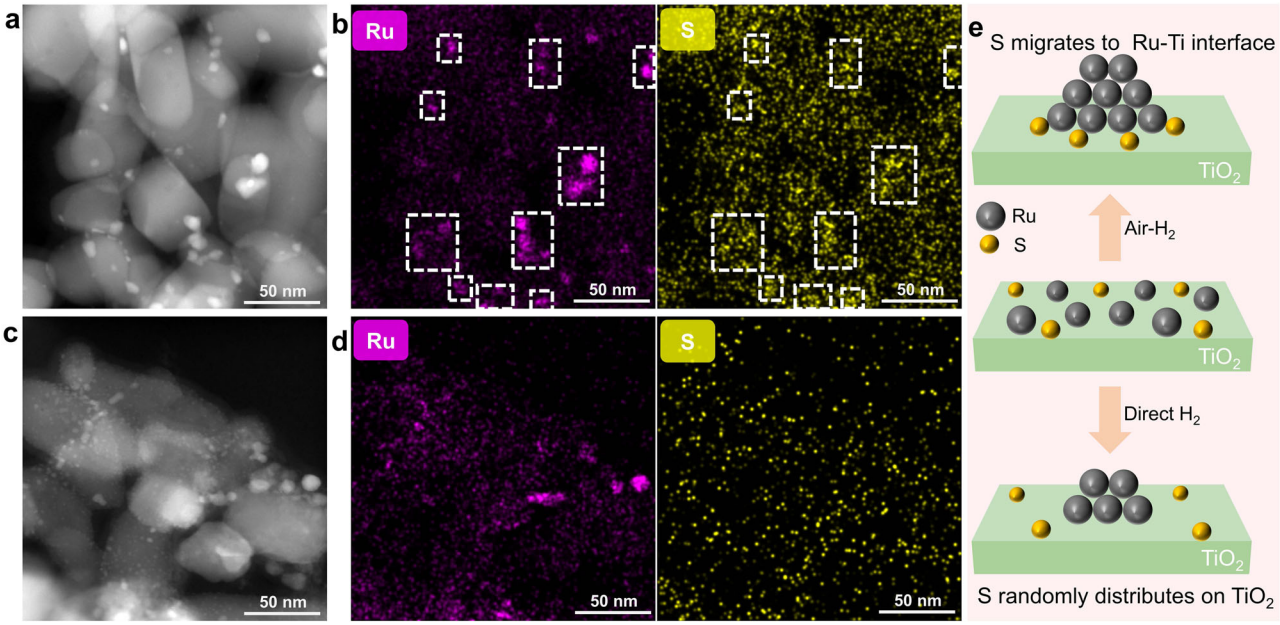

Fig. 2 | The geometric states of Ru NPs on TiO_2. a HAADF-STEM image of Ru/Ti-S-AR. **b** EDX mapping images of Ru and S elements on Ru/Ti-S-AR. **c** HAADF-STEM image of Ru/Ti-S-R. **d** EDX mapping images of Ru and S elements on Ru/Ti-S-R. **e** Schematic illustration of the evolution of Ru and S species on TiO_2 during air-H_2 or direct H_2 treatment.

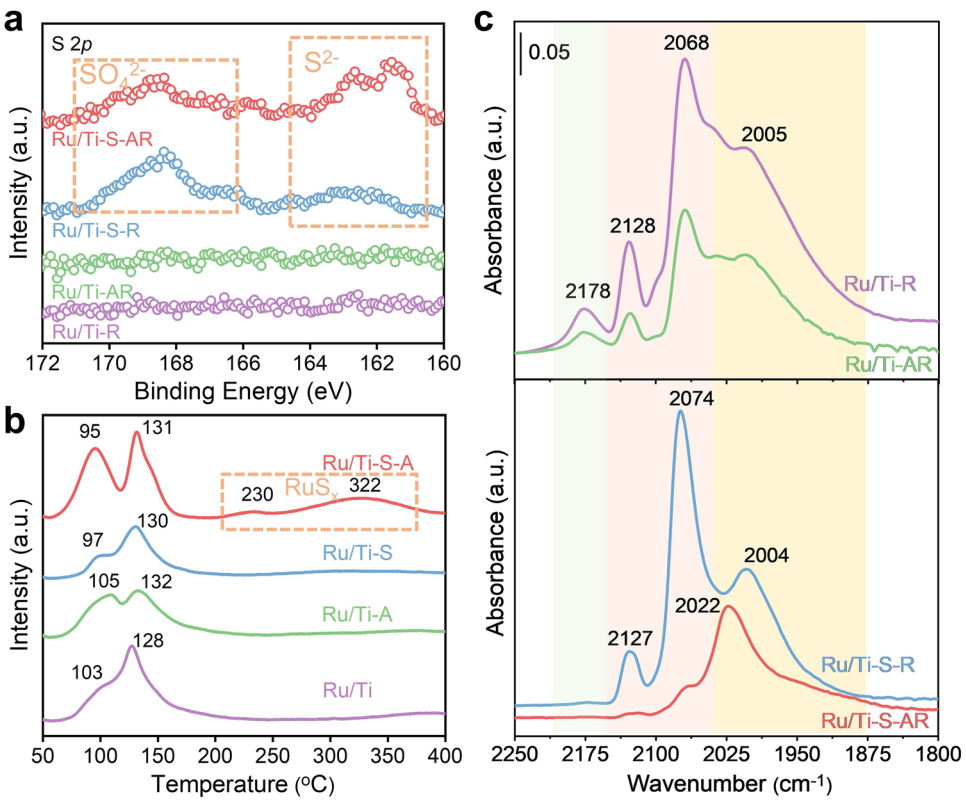

Fig. 3 | Characterization on the chemical states of S and Ru species in different catalysts. a S 2*p* XPS for Ru/Ti-S-AR, Ru/Ti-S-R, Ru/Ti-AR and Ru/Ti-R. **b** H_2-TPR profiles of Ru/Ti, Ru/Ti-A, Ru/Ti-S and Ru/Ti-S-A. **c** CO-DRIFTS on different catalysts at 25 °C, probing the surface states of Ru nanoparticles.

temperatures and exhibited H_2 reduction peaks at 128–131 °C. Furthermore, the ratio of interfacial RuO_x to surface RuO_x species in the Ru/Ti-S-R and Ru/Ti-R samples was noticeably higher than in the Ru/Ti-S-AR and Ru/Ti-AR samples. This observation could be attributed to the size difference of the Ru particles. The HAADF-STEM results showed that the Ru particles in the Ru/Ti-S-R and Ru/Ti-R samples were smaller compared to those in the Ru/Ti-S-AR and Ru/Ti-AR samples. Smaller Ru particles typically exhibited more interfacial RuO_x species on TiO_2, explaining the more abundant interfacial RuO_x in the Ru/Ti-S-R and Ru/Ti-R samples. Notably, the Ru/Ti-S-AR sample also displayed

two additional peaks at 230 and 322 °C, which were not observed on other samples. These peaks could be attributed to the reduction of RuS_x[30,31], formed due to the migration of sulfate to the Ru/TiO_2 interface during air annealing. This phenomenon resulted in a strong interaction between Ru and sulfate, leading to the presence of RuS_x peaks in H_2-TPR profile for Ru/Ti-S-AR sample.

To further investigate how the sulfate species induced the structural modification of Ru/TiO_2 catalyst, the chemical states of Ru were also characterized. The XPS results of Ru 3*d* for both Ru/Ti-AR and Ru/Ti-S-AR (Supplementary Fig. 14) revealed that the Ru species in the samples with or without sulfate were both in metallic state. Specifically, the presence of sulfate induced a slight shift of the metallic Ru peak from 279.7 to 279.9 eV, which might be due to the formation of Ru-S bonds at the Ru/TiO_2 interface[32]. For the impact of sulfate species on the structure TiO_2, no obvious changes were observed in Ti 2*p* on Ru/Ti-AR and Ru/Ti-S-AR (Supplementary Fig. 15), indicating that the presence of trace amount of sulfate species had negligible influence on the TiO_2 support, which was in line with the XRD and Raman results (Supplementary Figs. 12, 13).

To gain further insights into the surface states of Ru nanoparticles, we measured the CO adsorption at 25 °C using in situ diffuse-reflectance infrared Fourier transform spectroscopy (in situ DRIFTS). We firstly compared the CO adsorption on the sulfate-free Ru/Ti-R and Ru/Ti-AR samples. As shown in Fig. 3c, three CO vibrational bands at 2128, 2068, and 2005 cm^{-1} appeared after CO adsorption on the sulfate-free samples, corresponding to the adsorption of CO on different Ru sites. Specifically, the bands at 2128 and 2068 cm^{-1} could be assigned to the vibrations of CO on adsorbed on interfacial sites of Ru particles that interacted with the TiO_2[20,33], while the band at 2005 cm^{-1} could be ascribed to the characteristic of CO adsorbed CO on top sites of Ru particles that interacted with all surrounding sites by Ru-Ru bonds[18,33]. In addition, the bands at 2178 cm^{-1} could be ascribed to the CO adsorption on cationic Ti sites[34]. Notably, the intensities of the CO adsorption bands on Ru/Ti-AR were much lower than that on Ru/Ti-R, which could be due to the reduced exposure of Ru sites by air annealing. This observation was consistent with the HAADF-STEM results, which revealed that the Ru particle size in Ru/Ti-AR was apparently larger than that in Ru/Ti-R.

Next, the CO adsorptions on Ru/Ti-S-R and Ru/Ti-S-AR catalysts were examined. With the introduction of the sulfate to TiO_2, the CO adsorbed on TiO_2 (2178 cm^{-1}) nearly disappeared on Ru/Ti-S-R and Ru/Ti-S-AR, which should be due to the covering of cationic Ti sites by sulfate. In addition, the intensities of CO adsorption band associated with top sites of Ru particles (2004 cm^{-1}) and interfacial sites of Ru particles (2127 and 2074 cm^{-1}) on the Ru/Ti-S-R were comparable with the Ru/Ti-R, where only a very slight decrease was observed. This indicated that, during direct H_2 treatment, the introduced sulfate mainly stayed on TiO_2 and did not migrate to Ru particles. Notably, compared with the Ru/Ti-AR, the intensity of CO adsorption band (2127 and 2074 cm^{-1}) was dramatically decreased on the Ru/Ti-S-AR, implying that most interfacial sites of Ru particles were covered by sulfate. Meanwhile, CO adsorbed on top sites of Ru particles exhibited a shift to higher wavenumbers (from 2004 to 2022 cm^{-1}). This shift suggested an evolution of the top Ru atoms, in which the nearby interfacial Ru atoms occupied by sulfate might impact the Ru-CO bond of CO on top sites of Ru particles. The above results clearly showed that the sulfate on TiO_2 tended to migrate to Ru particles after air-H_2 treatment (Ru/Ti-S-AR), and did not migrate to Ru particles after direct H_2 treatment (Ru/Ti-S-R), which were consistent with the EDX mapping results.

Origin of the catalytic performance modification by the introduction of trace sulfates

It was usually considered that the activity and selectivity of CO_2 hydrogenation on supported Ru catalysts were affected by the size of Ru particles. Single Ru sites or small Ru clusters less than 1 nm were suggested to be selective for CO_2 hydrogenation to CO, while larger Ru particles were typically more active for methanation reaction[21,22]. Our HAADF-STEM results indicated that the presence of surface sulfate had little influence on the size distribution of Ru particles. Moreover, the valence state distribution of Ru species was not obviously affected either by the surface sulfate species (Supplementary Fig. 14). Therefore, the effects of Ru particle size and the Ru valence state related to sulfates on the catalytic performance could be excluded. The CO-DRIFTS data strongly suggested that the sulfate species significantly modified the interfacial Ru sites, which were likely the main active sites controlling the CO_2 conversion and product selectivity. It was reported that the activation of H_2 and the transfer of H were critical steps in CO_2 hydrogenation[23]. Our H_2-TPR results demonstrated that the H_2 activation on Ru particles occurred easily at low temperatures (<150 °C), indicating that the H_2 activation was not the rate-determining step. Recent reports indicated that the strong hydrogen spillover, associated with enhanced H and electron migration, could lead to the reduced activation of intermediate CO, subsequently resulting in the distinctly low CH_4 selectivity[18,23]. This suggested that the sulfate species modifying the interfacial Ru sites might significantly influence the migration of H and electrons, thus affecting the catalytic performance of Ru/TiO_2 catalyst for CO_2 hydrogenation.

We conducted a comprehensive in situ DRIFTS study of H_2 reactions with different samples to investigate the migration of H atoms and electrons. In this process, H_2 molecules dissociated into H atoms at metallic sites and spilled over to O sites on the surface of TiO_2 forming localized Ti-O(H)-Ti species. Simultaneously, the electrons were donated into the shallow trap states in the band gap of TiO_2, leading to a broad IR absorbance in the spectrum[23,35–37]. As shown in Fig. 4a, the introduction of H_2 at 523 K resulted in a very broad absorbance across the range of 4000 to 1000 cm^{-1} on Ru/Ti-S-AR, indicating the accumulation of electrons on the TiO_2 surface due to H_2 reduction. This broad IR absorbance was also observed on Au/TiO_2 and Rh/TiO_2, and it was attributed to the strong hydrogen spillover process[38,39]. In clear contrast, the Ru/Ti-R, Ru/Ti-AR, and Ru/Ti-S-R samples did not show such an adsorption feature, indicating that the intensity of hydrogen spillover on these samples was considerably lower than that on the Ru/Ti-S-AR. The temperature-dependent hydrogen spillover on Ru/Ti-S-AR was also depicted in Fig. 4b. As the temperature increased, the intensity of the broad absorbance across the range of 4000 to 1000 cm^{-1} was significantly enhanced, signifying that the hydrogen spillover was facilitated at higher temperatures. These findings demonstrated that the presence of sulfate species, which modified the interfacial Ru sites, greatly enhanced the hydrogen spillover process.

We next carried out DFT calculations to investigate how the sulfate modification induced changes in the H migration. Based on the experimental results presented earlier, the theoretical calculations primarily focused on H migration reactions occurring at perimeter sites between TiO_2 and Ru (Supplementary Figs. 16 and 17). The calculations revealed that the H migration from Ru to the bridge O of TiO_2 on the sulfate-free Ru-TiO_2 interface had a barrier of 1.91 eV and an endothermicity of 0.09 eV. In contrast, when the Ru/TiO_2 interface was modified by sulfate, this barrier decreased to 1.47 eV, and the reaction became exothermic with an energy release of 0.46 eV (Fig. 4c). This result suggested that the sulfate modification greatly enhanced the H transfer process at the Ru/TiO_2 interface.

During the CO_2 hydrogenation on Ru/TiO_2 catalysts, the general reaction mechanism involved the initial adsorption of CO_2 at the Ru-TiO_2 interface, accompanied by H_2 activation and dissociation to H on the Ru sites[9,11,20,40,41]. With the assistance of dissociated H, the adsorbed CO_2 could be activated to form intermediate CO[11,20]. The presence of sufficient H and electrons allowed the intermediate CO to further convert into CH_4. We performed DRIFTS studies under steady-state CO_2 hydrogenation conditions, and it was observed that CO_2 was easily

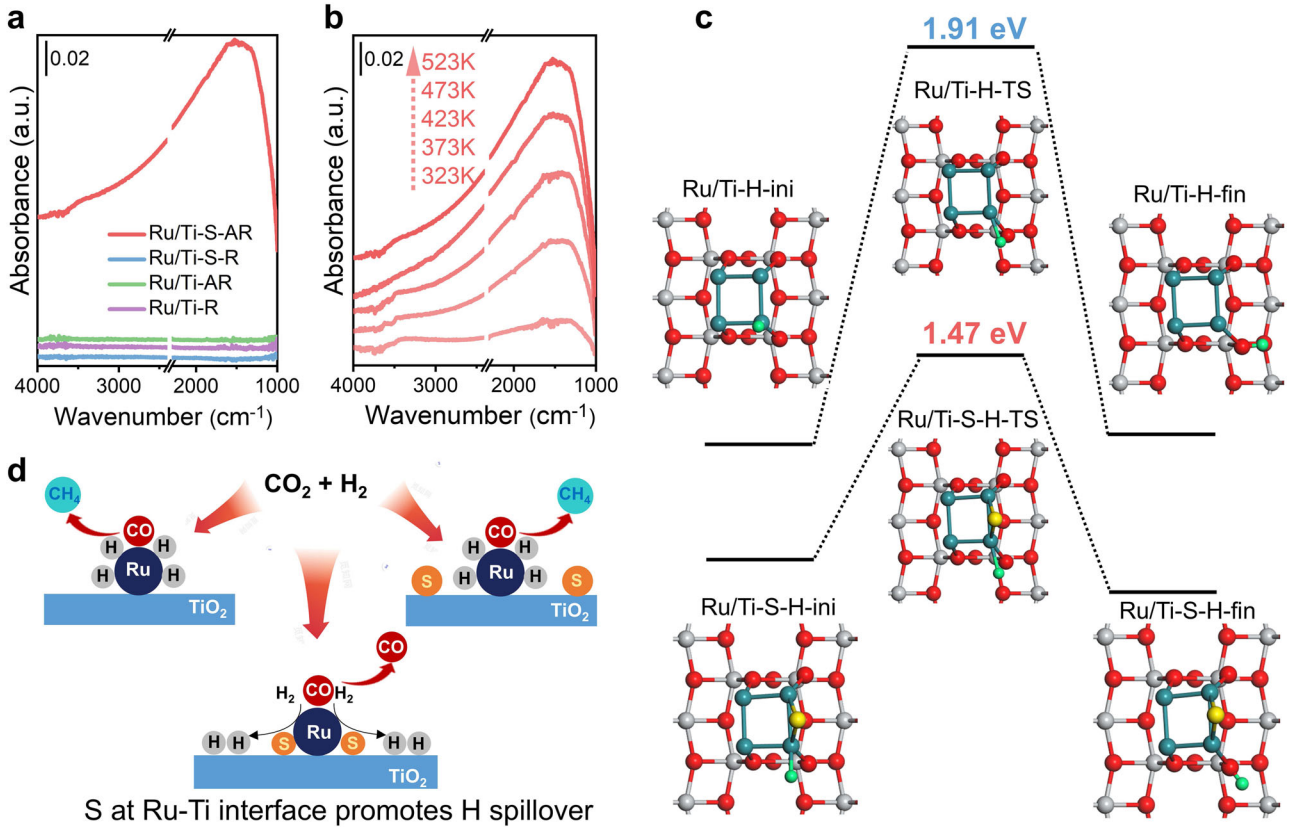

Fig. 4 | Revealing the origin of catalytic performance modification by trace sulfates. a In situ DRIFTS following the exposure to H_2 gas for Ru/Ti-S-AR, Ru/Ti-S-R, Ru/Ti-AR and Ru/Ti-R. **b** In situ DRIFTS following the exposure to H_2 gas for Ru/Ti-S-AR at different temperature. **c** DFT calculations of the H transfer process on sulfate-free and sulfate-containing Ru/TiO_2 catalysts (red, O; gray, Ti; cyan, Ru; yellow, S; green, H). **d** Schematic illustration of the mechanisms of CO_2 hydrogenation on sulfate-free and sulfate-containing Ru/TiO_2 catalysts.

converted to intermediate CO on Ru/Ti-AR and Ru/Ti-S-AR at low temperature. Additionally, the intermediate CO adsorbed at Ru site of Ru/Ti-AR could be converted to CH_4 when the reaction temperature was above 473 K, while the intermediate CO adsorbed at Ru site of Ru/Ti-S-AR was stable and no CH_4 was obtained (Supplementary Fig. 18). In the case of Ru/Ti-S-AR, where the Ru-TiO_2 interface was modified by sulfate, the H transfer process was greatly enhanced. This led to more H and electrons migrating from Ru to TiO_2 via the S medium, resulting in fewer H atoms remaining on the Ru sites. Consequently, this could effectively result in the low product selectivity to CH_4. In contrast, on the sulfate-free Ru/TiO_2, the hydrogen spillover and charge transfer could not proceed effectively. Therefore, the hydrogenation of adsorbed CO proceeded more smoothly, leading to the high CH_4 selectivity (Fig. 4d).

Catalytic performance can be remarkably affected, both advantageously and detrimentally, by the presence of trace impurities. However, the distinct significance of these trace impurities is often underestimated during the research process, which can potentially lead to erroneous conclusions. For example, sulfate, while capable of acting as a catalyst poison, can induce deactivation or reduced efficiency on some catalysts[42]. Conversely, on other types of catalysts, sulfate can play a positive role by enhancing metal dispersion or functioning as a promoter such as in photocatalytic water splitting for hydrogen production[43]. Other impurities such as chlorine, fluorine, or alkali cations can also yield similar positive or negative outcomes on catalytic performance[44–46]. In this work, the presence of trace amount of sulfate species on Ru/TiO_2 could significantly change the product distribution from high CH_4 selectivity to high CO selectivity. We also observed the similar product selectivity inversion by sulfate modification on other methanation catalysts such as the Rh/TiO_2 and Ni/TiO_2 catalysts (Supplementary Figs. 19, 20). These results further suggested the ubiquitous role of residual sulfate in controlling the product selectivity in the CO_2 hydrogenation. This groundbreaking discovery serves as a poignant reminder of the paramount importance of comprehending the intricate interplay between impurities and catalyst structure in the endeavor to design catalysts that are not only more efficient but also exhibit heightened selectivity. Researchers must account for the origin of impurities, control the impurity levels, and develop strategies to mitigate their disadvantageous effects while harnessing their positive impacts on catalytic performance.

Discussion

In summary, we discovered that the presence of residual sulfate species in commercial TiO_2 support, rather than the crystal structure of TiO_2, played a pivotal role in determining the product selectivity on the Ru/TiO_2 catalysts during CO_2 hydrogenation. Sulfate-free Ru/TiO_2 catalysts exhibited high CH_4 selectivity, whereas Ru/TiO_2 catalysts containing residual sulfate species displayed high CO selectivity. The annealing process in air at high temperatures induced the migration of sulfate on TiO_2 to the Ru/TiO_2 interface, where the interfacial sulfate species acted as an intermediate between the Ru sites and TiO_2 support, significantly promoting the H transfer from the former to the latter. The strong H spillover on Ru/TiO_2 catalysts containing residual sulfate species weakened the further activation of CO intermediates, resulting in low CO_2 conversion but very high selectivity to CO. These findings shed light on the role of trace impurities in heterogenous catalysis, and they can inform future research and development into ever more efficient and selective heterogeneous catalysts.

Methods

Syntheses of Ru/TiO_2 catalysts

Tetrabutyl titanate (TBOT, 99.5%) and ruthenium(III) nitrosyl nitrate were purchased from Aladdin. Commercial TiO_2 supports were purchased from Sigma-Aldrich and Aladdin. Ammonium sulfate was purchased from Beijing Innochem Science & Technology Co., LTD. TiO_2 were synthesized by hydrolyzing TBOT in a mixture of anhydrous ethanol and distilled water with a molar ratio of n(TBOT)/n(C_2H_5OH)/n(H_2O) = 1:15:4. Distilled water was dropped into the mixture of TBOT and anhydrous ethanol. The obtained precipitates were next dried and calcinated at 400 °C for 2 h. All Ru/TiO_2 catalysts with 5 wt.% Ru were prepared using the impregnation method. TiO_2 supports and a certain amount of $Ru(NO_3)_3$ were mixed in distilled water with stirring. The solution was evaporated at 60 °C under vacuum until dry. The resulting samples were dried at 100 °C overnight and then were calcined at 400 °C for 2 h in air or directly reduced with H_2 to prepare various Ru/TiO_2 catalysts. For the samples with sulfate addition, ammonium sulfate was incorporated during the impregnation process (with mole ratio of S/Ru set as 0, 0.03, 0.05, and 0.1).

Characterization

N_2 adsorption-desorption isotherms for the catalysts were measured at 77 K on a Quantachrome instrument. To remove the effects of other adsorbed species, all samples were degassed at 300 °C for 6 h under vacuum before the tests.

X-ray diffraction (XRD) analyses were performed on a Bruker D8 Advance diffractometer, using Cu Kα radiation (λ = 0.15406 nm) at 40 mA and 40 kV in the range 5° <2θ < 90° with a step size of 0.02°. The phase compositions of the catalysts were identified by comparison of the patterns with the Power Diffraction Files (PDF). The elemental analysis was performed using an inductively coupled plasma mass spectrometer (ICP-MS, Agilent 7700 s) equipped with a concentric nebulizer and a cyclonic spray chamber. High-angle annular dark field scanning transmission electron microscopy and element mapping images were taken by a JEOL JEM-ARM 200 F, operating at 200 kV.

X-ray photoelectron spectra measurements were carried out on an AXIS Supra instrument, using a standard Al Kα X-ray source (150 W) and a pass energy of 40 eV. The binding energies (BE) of spectra were adjusted by carbon calibration (C 1s = 284.8 eV).

H_2-temperature-programmed reduction (H_2-TPR) measurements were conducted using a Micromeritics Chemisorb 2920 analyzer. The samples (~100 mg) were placed into a U-shaped quartz tube and pretreated in an Ar (30 mL·min^{-1}) atmosphere at 300 °C for 0.5 h. Then the samples were heated from 50 to 800 °C at a heating rate of 15 °C·min^{-1} in a 10% H_2/Ar (50 mL·min^{-1}) flow. The effluent gas was passed through a cold trap to remove H_2O, and the signal was recorded by a thermal conductivity detector (TCD). For CO pulse chemisorption dispersion measurements, 70 mg of calcined catalyst was loaded into a U-shaped sample tube and reduced at 673 K for 1 h in 10% H_2/Ar. The catalyst was then flushed with He for 30 min. After cooling the sample to 323 K, pulse chemisorption measurements were performed with 10% CO/He while monitoring the effluent with a TCD.

In situ diffuse reflectance infrared Fourier transform spectroscopy (in situ DRIFTS) was performed on a Thermo Nicolet iS50 spectrometer equipped with a smart collector, and a liquid N_2-cooled MCT detector. The flow of the feed gas mixture was controlled using mass flow meters. All the spectra were measured with a resolution of 4 cm^{-1} and an accumulation of 32 scans. A background spectrum was subtracted from each spectrum. CO adsorption experiments were carried out at 50 °C, and the mixture gas contained 500 ppm of CO and N_2 balance at a total flow rate of 100 mL/min.

Spin-polarized DFT calculations were carried out using the Vienna Ab initio Software Package (VASP)[47]. The ion-electron interactions are described using the projector-augmented wave (PAW) method and Perdew–Burke–Ernzerhof (PBE) generalized gradient approximation (GGA) functional[48,49]. The TiO_2 anatase (101) surface was modeled with a slab consisting of three O-Ti-O layers and a 15 Å vacuum gap. The bottom layers were fixed to their bulk structure, while only the top layer was allowed to relaxed. The Ru/TiO_2 model was constructed according to previous reported literature[50]. A planewave with a cut-off energy of 400 eV was employed. Γ-point calculations were performed for geometry optimization, with the convergence criteria for the energy and force were set to 10^{-5} eV and 0.02 eV/Å, respectively. The transition states for H transfer reaction were identified by relaxing the force below 0.05 eV/Å via the climbing image nudged-elastic band (CINEB) method[51].

Catalytic tests

The evaluation of the CO_2 hydrogenation reaction was carried out in a quartz tube fixed-bed reactor under atmospheric pressure. The catalyst (50 mg) was loaded into the quartz tube and reduced with 10 vol.% H_2/N_2 (40 mL·min^{-1}) at 300 °C for 30 min prior to the catalytic performance evaluation. Then, the CO_2 hydrogenation reaction was performed at 250–550 °C under the reaction atmosphere of 4 vol.% CO_2, 16 vol.% H_2 and N_2 balance. The total flow rate was 40 mL·min^{-1}, and the gas hourly space velocity (GHSV) was 48,000 mL·h^{-1}·g_{cat}^{-1}. The outlet stream was analyzed by an online infrared gas analyzer. The experimental data variability for the activity tests was less than ±5%. CO_2 conversion in the activity test was defined as $([CO_2]_{inlet} - [CO_2]_{outlet})/[CO_2]_{inlet} \times 100\%$, and the selectivity for CH_4 and CO were calculated as $[CH_4]/([CH_4] + [CO]) \times 100\%$ and $[CO]/([CH_4] + [CO]) \times 100\%$, respectively.

Reporting summary

Further information on research design is available in the Nature Portfolio Reporting Summary linked to this article.

Data availability

Source data are provided with this paper.

References

1. Vogt, C. et al. Unravelling structure sensitivity in CO_2 hydrogenation over nickel. *Nat. Catal.* **1**, 127–134 (2018).
2. Zhang, X. et al. Product selectivity in plasmonic photocatalysis for carbon dioxide hydrogenation. *Nat. Commun.* **8**, 14542 (2017).
3. Dreyer, J. A. H. et al. Influence of the oxide support reducibility on the CO_2 methanation over Ru-based catalysts. *Appl. Catal. B Environ.* **219**, 715–726 (2017).
4. Ran, J. R., Jaroniec, M. & Qiao, S. Z. Cocatalysts in semiconductor-based photocatalytic CO_2 reduction: Achievements, challenges, and opportunities. *Adv. Mater.* **30**, 31 (2018).
5. Sastre, F., Puga, A. V., Liu, L. C., Corma, A. & Garcia, H. Complete photocatalytic reduction of CO_2 to methane by H_2 under solar light irradiation. *J. Am. Chem. Soc.* **136**, 6798–6801 (2014).
6. Neatu, S., Macia-Agullo, J. A., Concepcion, P. & Garcia, H. Gold-copper nanoalloys supported on TiO_2 as photocatalysts for CO_2 reduction by water. *J. Am. Chem. Soc.* **136**, 15969–15976 (2014).
7. Yuan, L. et al. Dynamic evolution of atomically dispersed Cu Species for CO_2 photoreduction to solar fuels. *ACS Catal* **9**, 4824–4833 (2019).
8. Yin, G. H. et al. Hydrogenated blue titania for efficient solar to chemical conversions: preparation, characterization, and reaction mechanism of CO_2 reduction. *ACS Catal* **8**, 1009–1017 (2018).
9. Li, S. et al. Tuning the selectivity of catalytic carbon dioxide hydrogenation over iridium/cerium oxide catalysts with a strong metal-support interaction. *Angew. Chem. Int. Ed.* **56**, 10761–10765 (2017).
10. Wang, F. et al. Active site dependent reaction mechanism over Ru/CeO_2 catalyst toward CO_2 methanation. *J. Am. Chem. Soc.* **138**, 6298–6305 (2016).

11. Kattel, S. et al. CO_2 hydrogenation over oxide-supported PtCo catalysts: The role of the oxide support in determining the product selectivity. *Angew. Chem. Int. Ed.* **55**, 7968–7973 (2016).
12. Cometto, C. et al. A Carbon nitride/Fe quaterpyridine catalytic system for photostimulated CO_2-to-CO conversion with visible light. *J. Am. Chem. Soc.* **140**, 7437–7440 (2018).
13. Chen, J. et al. Synergy between defects, photoexcited electrons, and supported single atom catalysts for CO_2 reduction. *ACS Catal* **8**, 10464–10478 (2018).
14. Wang, J. J. et al. A highly selective and stable ZnO-ZrO_2 solid solution catalyst for CO_2 hydrogenation to methanol. *Sci. Adv.* **3**, 10 (2017).
15. Kattel, S., Ramirez, P. J., Chen, J. G., Rodriguez, J. A. & Liu, P. Active sites for CO_2 hydrogenation to methanol on Cu/ZnO catalysts. *Science* **355**, 1296–1299 (2017).
16. Kattel, S., Liu, P. & Chen, J. G. G. Tuning selectivity of CO_2 hydrogenation reactions at the metal/oxide interface. *J. Am. Chem. Soc.* **139**, 9739–9754 (2017).
17. Wang, F. et al. Catalytic behavior of supported Ru nanoparticles on the (101) and (001) facets of anatase TiO_2. *RSC Adv.* **4**, 10834–10840 (2014).
18. Zhou, J. et al. Interfacial compatibility critically controls Ru/TiO_2 metal-support interaction modes in CO_2 hydrogenation. *Nat. Commun.* **13**, 327 (2022).
19. Wang, F. et al. Catalytic behavior of supported Ru nanoparticles on the {100}, {110}, and {111} facet of CeO_2. *J. Catal.* **329**, 177–186 (2015).
20. Chen, S. et al. Raising the CO_x methanation activity of a Ru/gamma-Al_2O_3 catalyst by activated modification of metal-support interactions. *Angew. Chem. Int. Ed.* **59**, 22763–22770 (2020).
21. Aitbekova, A. et al. Low-temperature restructuring of CeO_2-supported Ru nanoparticles determines selectivity in CO_2 catalytic reduction. *J. Am. Chem. Soc.* **140**, 13736–13745 (2018).
22. Kwak, J. H., Kovarik, L. & Szanyi, J. CO_2 reduction on supported Ru/Al_2O_3 catalysts: cluster size dependence of product selectivity. *ACS Catal.* **3**, 2449–2455 (2013).
23. Li, X. et al. Controlling CO_2 hydrogenation selectivity by metal-supported electron transfer. *Angew. Chem. Int. Ed.* **59**, 19983–19989 (2020).
24. Kim, A. et al. Selective CO_2 methanation on Ru/TiO_2 catalysts: unravelling the decisive role of the TiO_2 support crystal structure. *Catal. Sci. Technol.* **6**, 8117–8128 (2016).
25. Kim, C. et al. Energy-efficient CO_2 hydrogenation with fast response using photoexcitation of CO_2 adsorbed on metal catalysts. *Nat. Commun.* **9**, 8 (2018).
26. González-Castaño, M., Dorneanu, B. & Arellano-García, H. The reverse water gas shift reaction: a process systems engineering perspective. *React. Chem. Eng.* **6**, 954–976 (2021).
27. Zhang, Z., Wang, M., Zhou, H. & Wang, F. Surface sulfate ion on CdS catalyst enhances syngas generation from biopolyols. *J. Am. Chem. Soc.* **143**, 6533–6541 (2021).
28. Yu, M., Kosinov, N., van Haandel, L., Kooyman, P. J. & Hensen, E. J. M. Investigation of the active phase in K-promoted MoS_2 catalysts for methanethiol synthesis. *ACS Catal.* **10**, 1838–1846 (2020).
29. Panagiotopoulou, P. Methanation of CO_2 over alkali-promoted Ru/TiO_2 catalysts: II. Effect of alkali additives on the reaction pathway. *Appl. Catal. B Environ.* **236**, 162–170 (2018).
30. Infantes-Molina, A. et al. Role of Cs on hydrodesulfurization activity of RuS_2 catalysts supported on a mesoporous SBA-15 type material. *ACS Catal.* **1**, 175–186 (2011).
31. Castillo-Villalón, P. et al. Structure, stability and activity of RuS_2 supported on alumina. *J. Catal.* **260**, 65–74 (2008).
32. Li, J. et al. Distribution and valence state of Ru species on CeO_2 supports: support shape effect and its influence on CO oxidation. *ACS Catal.* **9**, 11088–11103 (2019).
33. Yan, Y. et al. Ru/Al_2O_3 catalyzed CO_2 hydrogenation: Oxygen-exchange on metal-support interfaces. *J. Catal.* **367**, 194–205 (2018).
34. Kots, P. et al. Electronic modulation of metal-support interactions improves polypropylene hydrogenolysis over ruthenium catalysts. *Nat. Commun.* **13**, 5186 (2022).
35. Chen, M. et al. Remarkable synergistic effect between {001} facets and surface F ions promoting hole migration on anatase TiO_2. *Appl. Catal. B Environ.* **207**, 397–403 (2017).
36. Chen, M. et al. Facet-dependent performance of anatase TiO_2 for photocatalytic oxidation of gaseous ammonia. *Appl. Catal. B-Environ.* **223**, 209–215 (2018).
37. Sheng, H. et al. Activation of water in titanium dioxide photocatalysis by formation of surface hydrogen bonds: An in situ IR spectroscopy study. *Angew. Chem. Int. Ed.* **54**, 5905–5909 (2015).
38. McEntee, M., Stevanovic, A., Tang, W., Neurock, M. & Yates, J. T. Jr. Electric field changes on Au nanoparticles on semiconductor supports-the molecular voltmeter and other methods to observe adsorbate-induced charge-transfer effects in Au/TiO_2 nanocatalysts. *J. Am. Chem. Soc.* **137**, 1972–1982 (2015).
39. Jeong, H. et al. Fully dispersed Rh ensemble catalyst to enhance low-temperature activity. *J. Am. Chem. Soc.* **140**, 9558–9565 (2018).
40. Kattel, S., Yan, B., Yang, Y., Chen, J. G. & Liu, P. Optimizing binding energies of key intermediates for CO_2 hydrogenation to methanol over oxide-supported copper. *J. Am. Chem. Soc.* **138**, 12440–12450 (2016).
41. He, Z. H. et al. Water-enhanced synthesis of higher alcohols from CO_2 hydrogenation over a Pt/Co_3O_4 catalyst under milder conditions. *Angew. Chem. Int. Ed.* **55**, 737–741 (2016).
42. Yin, P. et al. Sulfur stabilizing metal nanoclusters on carbon at high temperatures. *Nat. Commun.* **12**, 3135 (2021).
43. Kumar, S. G. & Devi, L. G. Review on Modified TiO_2 Photocatalysis under UV/visible light: Selected results and related mechanisms on interfacial charge carrier transfer dynamics. *J. Phys. Chem. A* **115**, 13211–13241 (2011).
44. Matsubu, J. C. et al. Adsorbate-mediated strong metal-support interactions in oxide-supported Rh catalysts. *Nat. Chem.* **9**, 120–127 (2016).
45. Zhang, C. et al. Alkali-metal-promoted Pt/TiO_2 opens a more efficient pathway to formaldehyde oxidation at ambient temperatures. *Angew. Chem. Int. Ed.* **51**, 9628–9632 (2012).
46. Liu, P. et al. Photochemical route for synthesizing atomically dispersed palladium catalysts. *Science* **352**, 797–801 (2016).
47. Kresse, G. & Furthmüller, J. Efficient iterative schemes for ab initio total-energy calculations using a plane-wave basis set. *Phys. Rev. B* **54**, 11169 (1996).
48. Grimme, S. Semiempirical GGA-type density functional constructed with a long-range dispersion correction. *J. Comput. Chem.* **27**, 1787–1799 (2006).
49. Kresse, G. & Furthmüller, J. Efficiency of ab-initio total energy calculations for metals and semiconductors using a plane-wave basis set. *Comput. Mater. Sci.* **6**, 15–50 (1996).
50. Zhang, S. et al. Density functional theory study on the metal-support interaction between Ru cluster and anatase TiO_2 (101) surface. *J. Phys. Chem. C* **118**, 3514–3522 (2014).
51. Henkelman, G. & Jónsson, H. Improved tangent estimate in the nudged elastic band method for finding minimum energy pathsand saddle points. *J. Chem. Phys.* **113**, 9978–9985 (2000).

Acknowledgements

This work was supported by the National Natural Science Foundation of China (22025604, 22276204) and the National Key R&D Program of China (2023YFC3708401). F.L. acknowledges the Startup Fund from the University of California, Riverside.

Author contributions

M.C. contributed to the central idea, performed the experiments, analyzed the data, and wrote the initial draft of the manuscript. L.L. performed the experiments. X.C., X.Q., and J.Z. contributed to data analysis. S.X. contributed to the manuscript revision. F.L. contributed to the refining of ideas, performing the analysis with constructive discussions, and manuscript revision. H.H. contributed to the project administration. C.Z. contributed to the funding acquisition, refining the ideas, carrying out additional analysis, and manuscript revision. All authors approved the final version of the manuscript.

Competing interests

The authors declare no competing interests.

Additional information

Supplementary information The online version contains supplementary material available at https://doi.org/10.1038/s41467-024-53909-8.

Correspondence and requests for materials should be addressed to Fudong Liu or Changbin Zhang.

Peer review information *Nature Communications* thanks the anonymous reviewers for their contribution to the peer review of this work. A peer review file is available.